J Fluoresc (2014) 24:239–250
DOI 10.1007/s10895-013-1291-x

ORIGINAL PAPER

# Luminescent Fluorene-Based Bis-Pyrazolyl Aniline Ligand for Aluminum Detection

**Andrew Frazer · Alma R. Morales · Adam W. Woodward · Paul Tongwa · Tatiana Timofeeva · Kevin D. Belfield**

Received: 4 June 2013 / Accepted: 21 August 2013 / Published online: 29 September 2013


**Abstract** The design, synthesis, and photophysical properties of a new fluorene-based fluorescent chemosensor, 4-((E)-2-(2-(benzo[d]thiazol-2-yl)-9,9-diethyl-9H-fluoren-7-yl)vinyl)-N,N-bis((3,5-dimethyl-1H-pyrazol-1-yl)methyl)benzenamine (**AXF-Al**), is described for the detection of $Al^{3+}$. **AXF-Al** exhibited absorption at 382 nm and strong fluorescence emission at 542 nm (fluorescence quantum yield, $\Phi_F$, of 0.80). The capture of $Al^{3+}$ by the pyrazolyl aniline receptor resulted in nominal change in the linear absorption (372 nm) but a large hypsochromic shift of 161 nm in the fluorescence spectrum (542 to 433 nm, $\Phi_F$=0.88), from which $Al^{3+}$ was detected both ratiometrically and colorimetrically. The addition of other metal ions, namely $Mg^{2+}$, $Ca^{2+}$, $Mn^{2+}$, $Fe^{2+}$, $Co^{2+}$, $Ni^{2+}$, $Cu^{2+}$, $Zn^{2+}$, $Cd^{2+}$, $Hg^{2+}$ and $Pb^{2+}$, produced only minimal changes in the optical properties of this probe. The emission band of this probe was also accessed by two-photon excitation in the near-IR, as two-photon absorption (2PA) is important for potential applications in two-photon fluorescence microscopy (2PFM) imaging. The 2PA cross section of the free fluorenyl ligand **AXF-Al** was 220 GM at 810 nm and 235 GM at 810 nm for the Al-ligand complex, practically useful properties for 2PFM.

**Keywords** Aluminum · Two-photon absorption · Fluorescence · Chemosensor · Probe · Ratiometric

A. Frazer · A. R. Morales · A. W. Woodward · K. D. Belfield
Department of Chemistry, University of Central Florida, Orlando, FL 32816-2366, USA

K. D. Belfield (✉)
CREOL, The College of Optics and Photonics, University of Central Florida, Orlando, FL 32816-2366, USA
e-mail: belfield@ucf.edu

P. Tongwa · T. Timofeeva
Department of Biology and Chemistry, New Mexico Highlands University, Las Vegas, NM 87701, USA

## Introduction

In the current climate, the public is becoming more aware of the importance of the monitoring and removal of harmful materials before and after they enter the biosphere. It is well accepted that aluminum targets the brain; hence, this element acts principally as a potent neurotoxin, with additional risk in the perinatal stage because of the more vulnerable neuronal tissue [1, 2]. There is also an abundance of research that has long linked this metal with Alzheimer's disease [3–5]. Data also supports $Al^{3+}$ acting as a toxic material for skin fibroblasts through the inhibition of superoxide dismutase, a material that plays an important role in skin exposed to oxygen as an antioxidant defense [6]. Bone is the major target tissue for the toxic effects of Al and is the primary site of Al accumulation [7], where it has been confirmed clinically, epidemiologically, and experimentally based on its capacity to induce two types of histological lesions, namely osteomalacia and adynamic bone disease [8].

Currently, the main analytical techniques used for the determination of $Al^{3+}$ are destructive and require an extraordinary amount of expertise for sample preparation. These include flame atomic absorption spectroscopy (FAAS) [9], electrothermal atomic absorption spectroscopy (AAS) [10], and inductively coupled plasma (ICP). There have also been some electrochemical tools available plus electroanalytical techniques, such as anodic stripping potentiometry (PSA) and anodic stripping voltammetry (ASV); this latter technique has high sensitivity, allowing for detection limits of parts per billion (ppb) [11]. Fluorometric techniques have been used in the detection of the aluminum ion, including single probes [12, 13] and nanoparticles [14], but it is still in its infancy compared to more mature areas such as mercury [15], zinc [15–17], and calcium probes [18].

The pursuit of selective and sensitive sensors able to monitor in real time and space the concentration of analytes of

biological, clinical, and environmental interest is generally accepted [19]. The ever-increasing demand for effective fluorescent chemosensors dictates that sensors must convert the event of analyte recognition by a receptor into an easily monitored and highly sensitive light signal from the chromophore reporter, which acts as a signaling unit [20]. The body of work to date is based on chromophores optimized for conventional (one-photon) fluorescence. A chief drawback of this design is that the excitation wavelengths are typically in the range of 350–560 nm, which may cause damage to the substrates [21]. This problem is averted by the development of two-photon chemosensors [22], which allow visualization of ions, small molecules, or even enzyme activity in living cells and tissue using 2PFM, a procedure that employs two near infrared (NIR) photons for excitation. Hence the impetus to develop new probes that have two large 2PA cross sections and high fluorescence quantum yields [23–26]. Two-photon excitation fluorescence (2PEF) further offers intrinsic 3D localization of a two-photon process (2PA) arising from the quadratic relationship of emission with excitation intensity; this limits excitation to a tiny focal volume and reduces background fluorescence [27]. Excitation occurs by up-conversion in the NIR region, so penetration depths are greater and photodamage to the matrix is minimized. In the case of biological tissues, the result is less phototoxicity coupled with the advantage of increased tissue depth. These inherent advantages have led to considerable effort now being made to synthesize new two-photon fluorescent (2PF) metal probes [28].

A number of ideas constituted the design structure of this probe. The fluorophore is based on the fluorenyl π-system, chosen due to its inherently high thermal and photochemical stabilities [29]. The unit can be readily functionalized in the 2, 7, and/or 9 positions, and, to date, we have worked diligently to optimize the synthesis and linear and nonlinear optical characterization of a number of fluorene derivatives with high 2PA [29, 30]. Recently, a number of these have been designed as successful probes in the targeting of cell organelles in the contemporary arena of two-photon bioimaging [28]. We also successfully developed probes for the detection of mercury and zinc ions [15, 16] and demonstrated their potential for use in bioimaging [17].

Here, we provide the description of the synthesis, structural characterization, and photophysical study of an aluminum ion detecting probe with a D–π–A construct based on a fluorenyl unit containing a benzothiazole motif as an electron acceptor group (A) and an aniline unit as an electron donor group (D). For the recognition moiety, we considered the chemistry of the polypyrazole ligands, which has developed quite rapidly over the last few decades; initiated by the late Trofimenko's introduction to scorpionates [31, 32]. The strong ability of pyrazole and its derivatives to serve as ligands has been the research subject of many coordination chemists, evident from the large number of articles in this area [33–37]. However, our search revealed no significant reference to any fluorescent metal sensors containing these ligands. The presence of metal ions in the same solution as other ions is common, so, when designing a chemosensor for metal detection, it is important to consider the relative sensitivity of the receptor to other metals. The aniline pyrazolyl unit's selectivity in the extraction of metals was an incentive to investigate this receptor attached to the chromophore [38, 39]. These design features ensure sensor reliability and multiple signaling properties, namely visible colorimetric and ratiometric properties.

Herein, we demonstrate the ability to selectively detect aluminum in the presence of other common ions. Quantitative assays to determine the concentration of analyte at a limit of 2.0 μM was also established. At low concentration of analyte, the probe acted as a reliable fluorescence sensor. Structural confirmation data, including single crystal x-ray crystallography, for this new molecule is also presented. The linear absorption, steady-state fluorescence, and fluorescence quantum yield ($\Phi_F$) of the probes were measured in solvents of different polarities to investigate possible solvatochromic effects. A series of titrations in ethanol of the selected solutions of metals with the probe at μM concentrations was tracked by steady state fluorescence, and the fluorescence quantum yield ($\Phi_F$) was calculated. The 2PA spectrum of the probe and complex were investigated using the two-photon excitation fluorescence (2PEF) method over a broad spectral range. The 2PA cross section ($\delta_{2PA}$) data indicated that this compound has potential as a two-photon absorbing metal probe for the detection of $Al^{3+}$ in 2PFM. The donor and acceptor units are spatially separated, so it will be possible to address HOMO and LUMO on binding with the cation. Quantum chemical calculations indicate the chromophore system displays preferential binding to the electron-deficient aluminum analyte.

## Experimental Section

2,7-Dibromo-9,9-diethylfluorene (**A**) [40], 7-bromo-9,9-diethylfluorene-2-carboxaldehyde (**B**) [41] and 2-(tributylstannyl)benzothiazole (**C**) [42] were prepared according to literature procedures. Reactions were carried out under $N_2$ or Ar atmosphere. THF was distilled over sodium benzophenone before use under a dry dinitrogen atmosphere [43, 44]. All other reagents and solvents were used as received from commercial suppliers. The $^1H$ and $^{13}C$ NMR measurements were performed using a Varian 500 NMR spectrometer with tetramethysilane (TMS) as an internal reference ($^1H$ referenced to TMS at $\delta = 0.0$ ppm and $^{13}C$ referenced to $CDCl_3$ at $\delta = 77.0$ ppm). FT-IR spectra were recorded on a Perkin Elmer spectrophotometer Model PE-1300 F0241. Elemental analyses were performed by Atlantic Microlab. High-resolution mass spectrometry (HR-MS)

analysis was performed at the Department of Chemistry, University of Florida, Gainesville, FL.

Synthesis of 7- Bromo-9, 9-Diethylfluorene-2-Carbaldehyde (**B**)

Under nitrogen atmosphere and at −78 °C, *n*-BuLi (3.28 mL, 1.6 M in hexanes) was added dropwise over 20 min to a dry THF solution (15 mL) containing 2,7-dibromo-9,9-diethylfluorene (2 g, 5.26 mmol). After 1 h of stirring, 0.58 mL of DMF was added slowly to the reaction solution. After another 2 h of stirring, the temperature of the solution was brought back to room temperature, and the reaction was quenched with 2 N HCl(aq). The solution was extracted with toluene and subjected to flash column chromatography (silica gel, hexanes/ethyl acetate 4:1). White solid was obtained (1.52 g, 89 % yield); mp 124–125 °C (lit. mp 126–128 °C) [41]. $^{1}$H NMR (500 MHz, $CDCl_3$) δ: 9.77 (s, 1H), 7.57 (s, 2H), 7.53 (d, $J$=7 Hz, 1H), 7.36 (d, $J$=8.5 Hz, 1H), 7.23−7.21 (m, 2 H), 1.83−1.72 (m, 4H), 0.3 (t, $J$=10 Hz, 6H) $^{13}$C NMR (126 MHz, $CDCl_3$) δ: 192.3, 153.5, 150.4, 146.8, 139.0, 135.6, 130.8, 130.4, 126.70, 126.4, 123.2, 123.1, 120.1, 56.7, 32.5, 8.5.

Synthesis of 2-(Tributylstannyl)Benzothiazole (**C**)

A THF solution (80 mL) of freshly distilled benzothiazole (9.90 g, 73.3 mmol) was cooled to −78 °C. To this was added *n*-BuLi (57 mL, 1.6 M) dropwise over 25 min to achieve a deep orange solution. $(n\text{-Bu})_3$SnCl (30.18 g, 92.72 mmol) was slowly added via syringe, and the reaction mixture was stirred at this temperature for another 30 min and then slowly bought up to −10 °C, where the reaction mixture was stirred for a further 30 min, and gradually allowed to warm to 0 °C, followed by the addition of aqueous KF (3 %, 50 mL), turning the reaction mixture bright yellow, followed by stirring an additional 1 h at 10 °C. The organic layer was then extracted with toluene and dried over anhydrous $MgSO_4$. After concentration under reduced pressure, the resulting orange liquid was purified by vacuum distillation at 144–146 °C/0.1 mmHg (lit. 144–146 °C at 0.15 mmHg) [42]. The yellow liquid was collected (72.80 g, 73 % yield). $^{1}$H NMR (500 MHz, $CDCl_3$) δ: 8.19–8.14 8.17 (dd, $J$=11.6, 8.2 Hz, 1H), 7.96 (dd, $J$=7.9, 1.9 Hz, 1H), 7.48−7.41 (m, 1H), 7.35 (m, 1H),), 1.67–1.58 (m, 6H), 1.40–1.23 (m, 12H), 0.94–0.86 (m, 9H). $^{13}$C NMR (126 MHz, $CDCl_3$) δ: 177.61, 156.11, 136.28, 125.26, 124.34, 122.78, 121.28, 28.87, 27.22, 13.62, 11.25.

Synthesis of 7-(Benzo[d]Thiazol-2-yl) -9,9-Diethyl-9H-Fluorene-2-Carbaldehyde (**D**)

7-Bromo-9,9-diethyl-9H-fluorene-2-carbaldehyde (9.4 g, 28.55 mmol) and 2-(tri-*n*-butylstannyl)benzothiazole (15 g, 35.39 mmol) were dissolved in 350 mL of toluene and degassed under vacuum and $N_2$. $Pd(PPh_3)_4$ (0.83 g, 0.1 mmol) was added, then the mixture was degassed for 25 min. The reaction mixture was heated to reflux under $N_2$. After 10 h, TLC revealed completion of the reaction. The black mixture was filtered through a short plug column. Toluene was removed in *vacuo*, and the resulting solid was filtered off and washed several times with hexane, affording 7.63 g of yellow crystals (7.63 g, 70 % yield); mp = 181–182 °C. $^{1}$H NMR (500 MHz, $CDCl_3$) δ: 10.09 (s, 1H), 8.19 (s, 1H), 8.13 (m, 2H), 7.94 (m, 5H), 7.54 (t, $J$=7.5 Hz, 1H), 7.43 (t, $J$=7.5 Hz, 1H), 2.22 (m, 4H), 0.36 (t, $J$=7.5 Hz, 6H). $^{13}$C NMR (126 MHz, $CDCl_3$) δ: 192.1, 168.0, 154.1, 152.2, 151.4, 146.7, 142.7, 135.9, 135.0, 133.9, 130.5, 127.4, 126.5, 126.4, 125.4, 125.2, 123.3, 121.6, 121.4, 120.6, 56.7, 32.6, 32.5, 8.5, 8.5. HRMS-ESI $C_{25}H_{21}NOS$ theoretical m/z $[M+H]^+$ = 384.1422, found 384.1408; theoretical m/z $[M+Na]^+$ = 406.1236, found 406.1220.

Synthesis of Diethyl (4-(bis((3,5-Dimethyl-1H-Pyrazol-1-) Methyl)Amino)Phenyl)Methylphosphonate (**G**)

A ground mixture of (3,5-dimethyl-1H-pyrazol-1-yl)methanol (1.03 g, 8.23 mmol) and diethyl (4-aminophenyl) methylphosphonate (0.50 g, 2.06 mmol) was prepared in a flask equipped with a Dean-Stark condenser. This mixture was then heated and held at a melt temperature of 80 °C for 12 h, followed by $^{1}$H NMR monitoring. The excess pyrazole was then removed by sublimation and the remaining product was washed with hexanes (3×20 mL) and dried under vacuum, revealing white solid (0.80 g, 85 % yield); mp = 89–91 °C. $^{1}$H NMR (500 MHz, $CDCl_3$) δ: 7.16 (d, 2H), 6.99 (d, 2H), 5.72 (s, 2H, $H(pz_{(H4)})$, 5.48 (s, 4H, $CH_2$-pz), 3.97(m, 4H), 3.07 (d, 2H), 2.18 (s, 6H), 2.03 (s, 6H), 1.21 (t, 6H). $^{13}$C NMR (126 MHz, $CDCl_3$) δ: 147.8, 145.3, 139.4, 130.4, 125.7, 121.0, 105.7 ($pz_{(C4)}$), 64.3 ($CH_2$-pz), 62.0, 33.5, 32.4, 16.4, 13.6, 11.0. HRMS-ESI $C_{23}H_{34}N_5O_3P$ theoretical m/z $[M+H]^+$ = 460.2472, found m/z $[M+H]^+$ = 460.2458; theoretical m/z $[M+Na]^+$ = 482.2291, found m/z $[M+Na]^+$ = 482.2313.

Synthesis of the Probe 4-((E)-2-(2-(Benzothiazol-2-yl) -9,9-Diethyl-9H-Fluoren-7-yl)Vinyl) -N,N-bis((3,5-Dimethyl-1H-Pyrazol-1-yl)Methyl) Benzenamine (**AXF-Al**)

To a THF solution (10 mL) of diethyl (4-(bis((3,5-dimethyl-1H-pyrazol-1-yl)methyl)amino)phenyl)methylphosphonate (**G**) (0.24 g, 0.52 mmol) at −78 °C was added powdered *t*-BuOK (0.13 g, 1.16 mmol), resulting in an immediate color change to pale yellow. After 30 min, the reaction mixture was warmed to 0 °C and stirred for another 30 min at this temperature. 7-(Benzo[d]thiazol-2-yl)-9,9-diethyl-9H-fluorene-2-

carbaldehyde (**D**) (0.15 g, 0.39 mmol) was then added, producing a red reaction mixture, which was stirred for a period of 18 h. The reaction mixture was then quenched with water, followed by extraction with dichloromethane. This was then dried over anhydrous $Na_2SO_4$ and the volatiles removed to reveal crude yellow solid. The crude product was purified by column chromatography on silica gel, eluting with a 1 % $Et_3N$ solution of EtOAc/hexanes 3:2, affording yellow powder (0.17 g, 63 % yield); mp = 139–140 °C. $^1$H NMR (500 MHz, $CDCl_3$) δ: 8.13 (s, 2H), 8.10−8.08 (d, 2H, $J$= 10 Hz), 8.03−8.02 (m, 2H), 7.92−7.90 (d, 2H, $J$=10 Hz), 7.78 −7.70 (m, 4H), 7.51−7.47 (m, 6H), 7.42−7.39 (d, 2H, $J$= 15 Hz), 7.39−7.36 (t, 3H, $J$=5 Hz), 7.10−7.09 (d, 1H, $J$= 5 Hz), 7.07−7.06 (d, 1H, $J$=5 Hz), 5.76 (s, 2H, **H**$_{(pzH4)}$), 5.54 (s, 4H, C**H**$_2$-pz), 2.21 (s, 6H), 2.08 (s, 6H), 1.25 (t, 4H), 0.37 (q, 6H). $^{13}$C NMR (126 MHz, $CDCl_3$) δ: 171.3, 168.9, 151.4, 151.2, 148.1, 144.6, 139.7, 137.7, 132.4, 128.2, 127.6, 127.6, 127.4, 126.5, 125.9, 125.2, 123.2, 121.8, 121.7, 120.8, 120.7, 120.4, 120.2, 106.1(pz$_{(C4)}$), 64.2 (**C**H$_2$-pz), 60.6, 58.4, 56.6, 56.6, 33.0, 21.3, 13.8, 11.3, 8.8. Anal. Calcd. For $C_{49}H_{54}N_6O_2S$ (**AXF-Al**+1 mole of EtOAc); 74.40; H, 6.88; N, 10.62; Found: C, 74.03; H, 6.88; N, 10.86. HRMS-ESI theoretical m/z $[M+H]^+$ = 689.3421, found m/z $[M+H]^+$ = 689.3449; theoretical m/z $[M+Na]^+$ = 711.3240, found m/z $[M+Na]^+$ = 711.3270.

## X-Ray Structural Analysis

The crystal data, details of the data collection, and structure refinement parameters for compound **AXF-Al** are presented in Tables 1 and 2. A single crystal X-ray diffraction experiment was carried out using a Bruker SMART APEX II diffractometer with a CCD area detector (graphite monochromated Mo $K_\alpha$ radiation, $\lambda$=0.71073 Å) using $\Theta$-scans with a 0.5° step in ω at 100 K. The semi-empirical SADABS method was applied for absorption correction. The structure was solved by direct methods and refined by the full-matrix least-squares technique against $F^2$ with the anisotropic temperature parameters for all non-hydrogen atoms. All hydrogen atoms were placed geometrically and refined in a riding model. Data reduction and further calculations were performed using Bruker SAINT+ and SHELXTL NT program packages.

**Table 1** Photophysical data for **AXF-Al** in solvents with varying polarities

| Solvent | $\lambda_{max}{}^{abs}$/nm | $\lambda_{max}{}^{em}$/nm | Stokes shift/nm | QY |
|---|---|---|---|---|
| Chloroform | 386 | 498 | 112 | 1.0 |
| DMSO | 395 | 571 | 176 | 0.89 |
| THF | 391 | 503 | 112 | 0.91 |
| EtOH | 382 | 542 | 160 | 0.80 |

**Table 2** Summary of the crystal data and structure refinement parameters for **AXF-Al**

| Compound | AXF-A1 |
|---|---|
| Empirical formula | $C_{48}H_{52}N_6O_2S$ |
| FW | 777.02 |
| T, K | 100(2) |
| Crystal size, mm | 0.40×0.30×0.20 |
| Crystal system | Triclinic |
| Space group | P-1 |
| $a$, Å | 10.328(3) |
| $b$, Å | 14.347(5) |
| $c$, Å | 14.725(11) |
| $\alpha$, deg. | 91.127(4) |
| $\beta$, deg. | 106.622(3) |
| $\gamma$, deg. | 93.641(4) |
| $V$, Å$^3$ | 2084.8(11) |
| $Z$ | 2 |
| $d_c$, g cm$^{-3}$ | 1.238 |
| $F$(000) | 828 |
| $\mu$, mm$^{-1}$ | 0.125 |
| $2\theta_{max}$, deg. | 60.94 |
| Index range | −14<=$h$<=14 |
| | −20<=$k$<=20 |
| | −20<=$l$<=20 |
| No. of rflns collected | 33189 |
| No. of unique rflns | 12568 |
| Data/restraints/parameters | 12568/0/514 |
| $R1$; $wR2$ ($I>2\sigma(I)$) | 0.0643; 0.1639 |
| $R1$; $wR2$ (all data) | 0.1076; 0.1874 |
| GOF on $F^2$ | 1.022 |
| $T_{min}$; $T_{max}$ | 0.9403; 0.9755 |

## General Instrumental Information

UV–vis absorption spectra were obtained using an Agilent 8453 UV-Visible spectrophotometer and 1.0 cm path lengths quartz cuvettes. Fluorescence emission spectra were obtained with a PTI QuantaMaster spectrofluorimeter with a 75-W continuous Xe-arc lamp as a light source.

## Determination of Quantum Yields

The quantum yield of the sample was obtained through a comparison of the integrated area of the corrected emission spectrum of the sample with that of a known standard, such as 9,10-diphenylanthracene ($\phi$=0.95 in cyclohexane). The quantum yield of the sample was calculated from Eq. 1 [45].

$$\phi = \phi_r \cdot \frac{I}{I_r} \cdot \frac{OD_r}{OD} \cdot \frac{n^2}{n_r^2} \quad (1)$$

Where $I$ and $I_r$ are the corrected integrated fluorescence intensity of the sample and the standard; $OD$ and $OD_r$ are the optical density (absorbance) of the sample and the standard; $n$ and $n_r$ are the refractive index of the sample and the standard, respectively.

## Anisotropy

Excitation anisotropy spectra were measured using two polarizers in the L-format method, with correction for background signals, in high-viscosity solvents (polytetrahydrofuran and glycerol) at room temperature [46]. The experimental details of anisotropy measurements were previously reported [47–49].

## Determination of Two-Photon Absorption Cross Sections, δ

The degenerate 2PA spectra of probe and metal-ligand complexes were measured in EtOH over a broad spectral region by the relative 2PF method [50]. Rhodamine B in methanol, whose comprehensive characterization has been reported [46] was used as a standard. Two-photon-induced fluorescence spectra were obtained with a PTI QuantaMaster spectrofluorimeter coupled with a mode-locked Coherent Mira 900 laser system. The pulse width of the laser was 200 fs with a repetition rate of 76 MHz and 700 mW average power. Fluorescence measurements were performed in 10 mm fluorometric quartz cuvettes with dye concentrations ~$4\times10^{-5}$ M. The values of 2PA cross sections, $\delta_{2PA}$, were determined by Eq. (2).

$$\delta_t = \delta_r \cdot \frac{\langle F_t\rangle n_t^2 C_r \Phi_r P_r^2}{\langle F_r\rangle n_r^2 C_t \Phi_t P_t^2} \quad (2)$$

Where, $r$ and $t$ describe the reference and the tested sample, respectively; $<F>$ is the average fluorescence intensity integrated from the 2PF spectrum; $n$ is the refractive index of the solvent; $C$ is the concentration; $\Phi$ is the quantum yield; and $P$ is the incident power in the sample.

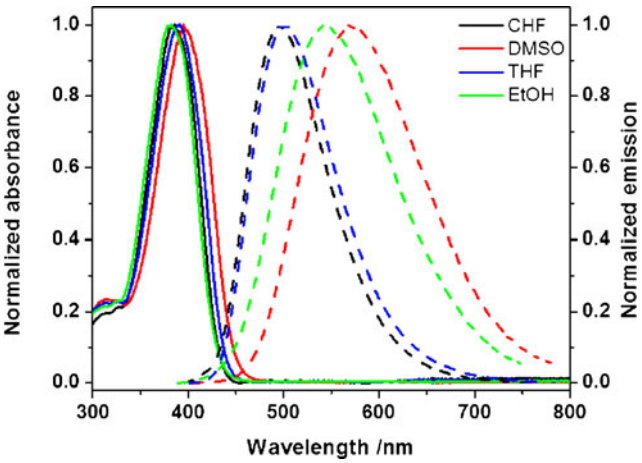


**Fig. 1** Normalized absorbance (*solid line*) and emission spectra (*dashed line*) of **AXF-Al** in the presence of solvents with varying polarities

## UV–Vis Absorption and Fluorescence Emission Titration Procedure

The steady-state absorption and fluorescence emission spectra of the probe were investigated in $CHCl_3$, EtOH, DMSO, and THF with concentrations ≥$2\times10^{-6}$ M at room temperature in 1 cm quartz cuvettes using an Agilent 8453 UV-visible spectrophotometer and PTI Quantamaster spectrofluorimeter, respectively. All solvents and solutions used in these experiments were checked for spurious emissions in the region of interest and purged with $N_2$ gas for 20 min prior to spectroscopic measurements. The concentrations did not exceed $2\times10^{-6}$ M, so processes of reabsorption were negligible. UV–vis absorption and fluorescence emission titrations were performed in EtOH. A 3.0 mL aliquot of dye solution was prepared and the corresponding metal ion stock solution was added. The resulting solution was agitated and recorded via

**Scheme 1** Synthesis of the fluorene-based aluminum probe **AXF-Al**

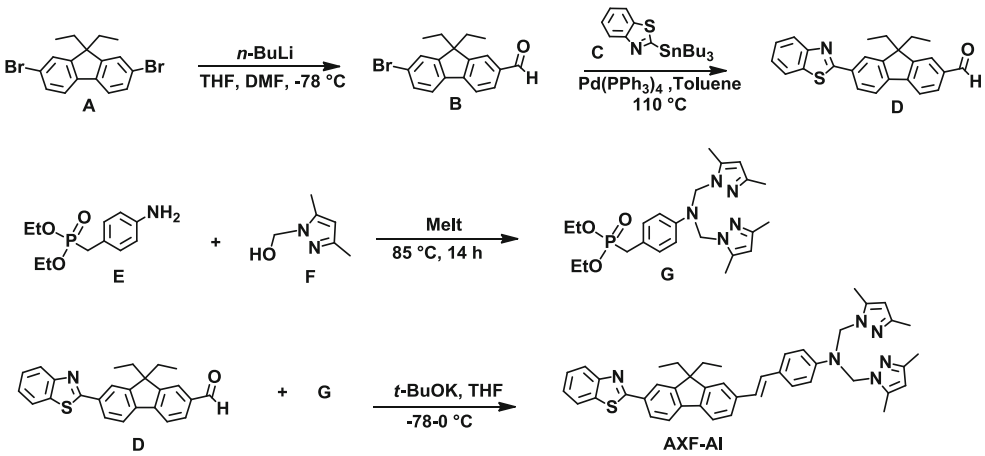

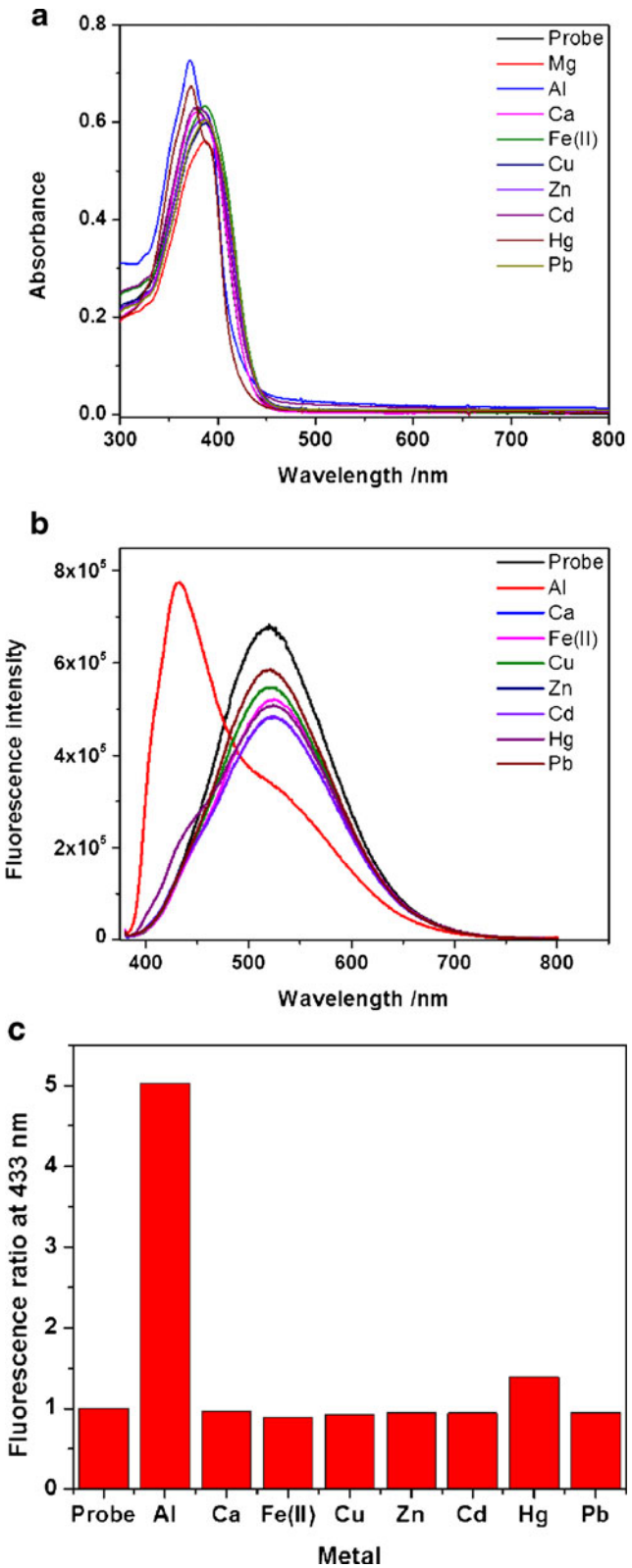


**Fig. 2** Absorbance (**a**) and fluorescence (**b**) response of various metal ions relative to **AXF-Al** at 4 μM concentration in EtOH; (**c**) ratio of emission from complex to that of the ligand at 433 nm

UV–vis absorption and fluorescence emission spectra. Experiments were performed in triplicate.

### Determination of the Stoichiometry Number of the Complex

The basic Eqs. (3–5) for the determination of the ligand-metal complexation are

$$D + nM \rightleftharpoons C \tag{3}$$

Where D is the dye molecule (ligand), M is the metal ion, and C is the complex.

### Calculation of the Binding Constants

The binding constant, $K$, of the metal complex was determined from Eq. 4 with the approximation the concentration of the free metal is equal to its total concentration ([M] ≅ $[M]_t$) [51–53].

$$\frac{F-F_0}{F_m-F} = \frac{[C]}{[D]} = K[M]^n \tag{4}$$

Where $F_o$, F, and $F_m$ are the corrected fluorescence emission intensity of the complex at initial, interval t, and the final state at which the complex was fully formed upon the addition of metal ion, respectively. Binding constant $K$ can be determined from the plot of the linear regression of log[(F-$F_0$)/($F_m$-F)] against log[M] in Eq. (5) that is derived from Eq. 4 to obtain the intercept as log $K$ and the slope $n$.

$$\log\left(\frac{F-F_0}{F_m-F}\right) = \log K + n \log[M] \tag{5}$$

## Results and Discussion

The strategy from the outset in designing this probe was based on a stable fluorenyl core. The synthesis of the chromophore is

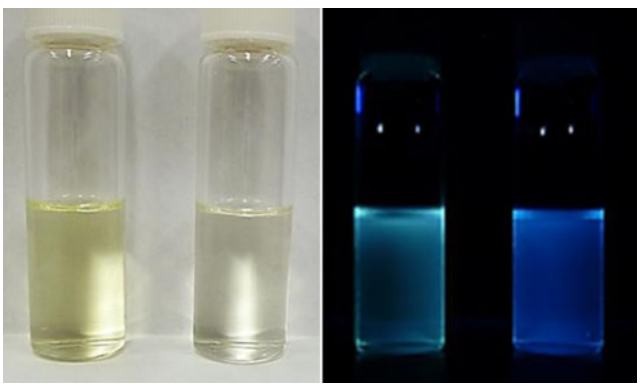

**Fig. 3** Sample of **AXF-Al** (2 μM in EtOH) before (left vial) and after (right vial) treatment with molar equivalent $Al^{3+}$ with white light (left figure) and under 365 nm UV excitation (right figure)

presented in Scheme 1. Ethyl groups in the fluorenyl 9-position were used to enhance solubility. One of the key starting materials was the benzothiazole fluorenyl aldehyde (**D**), synthesized by an efficient Stille coupling reaction starting from the bromofluorene aldehyde (**B**) and tri-*n*-butyltinbenzothiazole (**C**) in good yield, 72 % (Scheme 1). This is an improvement on past literature, which reported condensation of a fluorene-2,7-dicarbaldehyde with a mole equivalent of o-thioaniline.[29, 54] Methyl pyrazolyl aniline diethylphosphonate (**G**) was successfully synthesized using solvent-free condensation of the (3,5-dimethyl-1H-pyrazol-1-yl)methanol (**F**) with the commercially available diethyl 4-aminobenzylphosphonate (**E**) in a melt reaction. The incorporation of a styryl group directly connected to the π-bridge was employed to increase the conjugation of the chromophore, achieved by the Horner-Wadsworth-Emmons olefination of the resulting phosphonate, carried out in THF as a solvent with potassium *t*-butoxide as the base [55, 56].

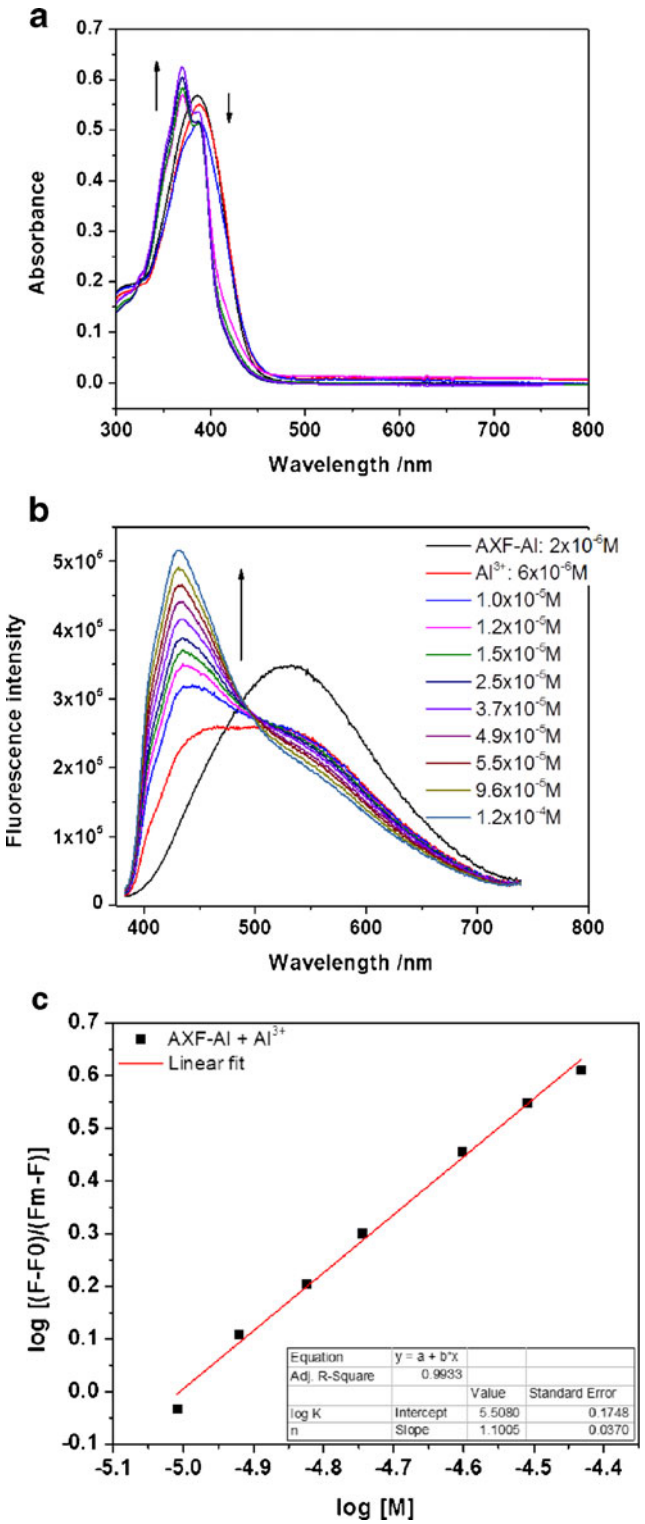


**Fig. 4** (**a**) Absorbance spectra showing response of the titration of $Al^{3+}$ with probe (2 μM in EtOH); (**b**) fluorescence response of the titration of $Al^{3+}$ with probe (2 μM in EtOH); (**c**) determination of binding constants for probe with $Al^{3+}$ using a linear regression plot of log $[(F\text{-}F_0)/(F_m\text{-}F)]$ vs. log $[Al^{3+}]$, Eq. 2 correlation coefficient of $r = 0.9932$

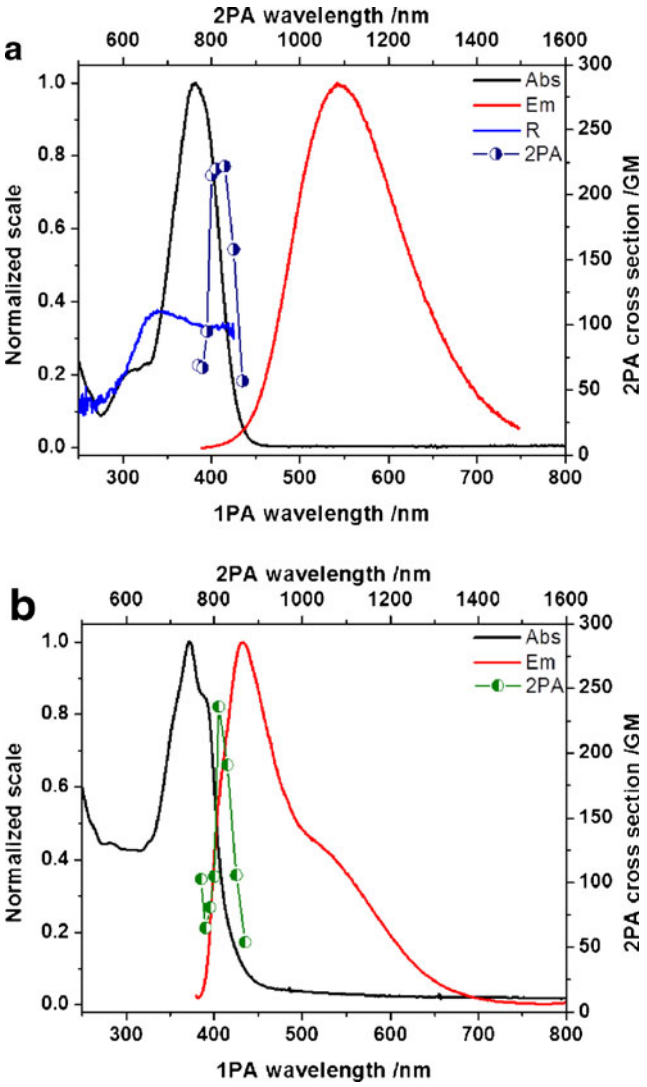


**Fig. 5** (**a**) Absorption (*black*), emission (*red*), and 2PA (*green semi-circles*) spectra of the probe in EtOH and anisotropy (*blue*) in glycerol; (**b**) absorption (*black*), emission (*red*), and 2PA spectra (*green semi-circles*) of the equilibrium complex (probe-Al complex) in ethanol

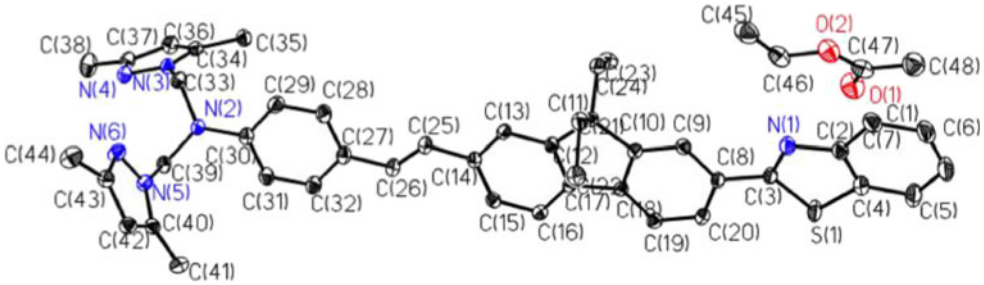


**Fig. 6** ORTEP drawing for **AXF-Al** with the numbering scheme. Thermal ellipsoids are shown with the 50 % probability level. Hydrogen atoms have been omitted for clarity

The probe was isolated as an air-stable solid with good solubility in a variety of solvents.

## Selectivity and Optical Properties of the Chemoselective Probe

The UV absorption and emission spectra of the probe showed a typical bathochromic shift with increasing solvent polarity (Fig. 1). The fluorescent enhancement effect of **AXF-Al** in EtOH was investigated by excitation at $\lambda_{ex}$=375 nm, and the fluorescence response of the probe to various cations and its selectivity for $Al^{3+}$ were recorded, as shown in Fig. 2. Ethanol was chosen as the solvent as it served to solvate both the ligand and the metal salts, as well as providing a similarity to an aqueous environment. The fluorescence spectral changes were monitored upon interaction with 2 μM EtOH solutions of the targeted metal perchlorates. No significant spectral changes were observed for the probe in the presence of group 12 congeners ($Zn^{2+}$ and $Cd^{2+}$), first-row transition metals ($Fe^{2+}$ and $Cu^{2+}$), and environmentally important metals ($Hg^{2+}$ and $Pb^{2+}$), plus alkaline earth metals ($Ca^{2+}$ and $Mg^{2+}$); see Fig. 2a and b. The experimental results suggest that this molecule has notable selectivity toward $Al^{3+}$ (Fig. 2c), and the response is visible to the naked eye (Fig. 3).

The UV–vis absorption spectra of the probe and its interaction through titration with $Al^{3+}$ (Fig. 4a) were measured in EtOH solutions. The probe exhibited a peak absorption at 382 nm and a gradually blue-shift upon the sequential addition of $Al^{3+}$ (Fig. 4b). A selective ion probe that gives a positive response rather than fluorescent quenching upon analyte binding is usually preferred to promote sensitivity. The emission spectra of the free ligand titrated with $Al^{3+}$ (Fig. 4b) resulted in the appearance of a new fluorecence band at 432 nm, shifted from 532 nm for the pure ligand. This decrease in wavelength upon binding suggests that the relaxation energy from the excited state is larger for the complex than for the unbound ligand. The large 100 nm hypsochromic shift could be attributed to a reduction in intermolecular charge transfer (ICT) [57]. This dramatic result found with $Al^{3+}$ and the probe may be a consequence of the size and polarizability of the $Al^{3+}$ ion.

The $Al^{3+}$ is believed to interact strongly with the pyrazolyl nitrogens and, even though the resulting molecular assemblies are unknown, it is believed to restrict the excited state vibrations of the chromophore, resulting in an increase in fluorescence properties [58]. A single set of isobestic points was observed in both the absorption and emission spectra, suggesting a single equilibrium was reached in complexation.

## Binding Constant of Metal Complex

The binding constant $K$ for the probe with $Al^{3+}$ was calculated from the titration curve (Fig. 4c). It revealed a 1:1 ratio of the ligand with aluminum in the complex at equilibrium. These results are comparable to those reported for the 1:2 complexation of ligand to metal for a 1:2 zinc-butylcalix [4]arene [59], a cobalt-quercetin [60], a lithium-anthraquinone cryptand [61]. A binding constant of log $K$=5.5 was determined by linear fitting using Eq. 5. For both biochemical and environmental sensing, a successful metallo-responsive fluorophore would need a high binding constant to ensure detection limits in the parts-per-billion range [62]. Tentatively, we assume that the smaller ion binds with the dimethyl pyrazole chelate present in the ligand, thus resulting in a 1:1 assembly that engages the tridenticity of the ligand. This would result in the direct coordination of the aniline nitrogen to the metal. As the donating ability of the aniline nitrogen to the extended chromophore decreases, we see a reduction in the intramolecular charge transfer (ICT), reflected in the blue shift on binding.

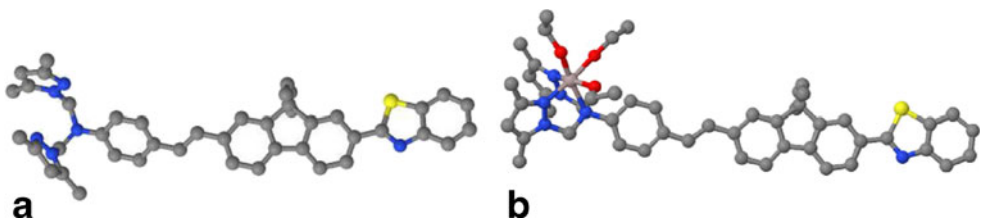


**Fig. 7** Optimized geometries for **AXF-Al** (**a**) and the probe-aluminum complex (**b**)

Nonlinear Spectroscopy

Two-photon absorption cross sections ($\delta_{2PA}$) of the probe and its complex with aluminum were determined over a broad spectral region, 740–900 nm, using a two-photon-induced fluorescence measurement technique [46] in EtOH. 2PA of the complex was measured using a probe/$Al^{3+}$ ratio of 1:1. Figure 5 shows the 2PA spectrum, with maxima 220 GM at 810 nm and 235 GM at 810 nm for the probe **AXF-Al** and the metal complex respectively. The long wavelength 2PA band is close to the 1PA band, which is typical of an unsymmetrical fluorene derivative [63]. This change in the $\delta_{2PA}$ of the aluminum complex is nominal when compared with ligand. Well-defined long wavelength 2PA bands in the spectral range of one-photon allowed transitions are associated with the relatively large changes in the stationary dipole moments of the ligand and ligand-metal complex ($|\Delta\mu|$~5–10 D) under the $S_0 \rightarrow S_1$ electronic excitation [64]. The 2PA process is a third-order nonlinear optical property with a strong dependence on the intramolecular charge transfer (ICT) process [65]. The architecture of this dye promotes the strong 2PA cross sections observed in linear conjugated molecules with D-π-A motif, which is contingent on the electronic contribution of the donor. A stronger donor will enhance the charge transfer process and, thus, increase the transition dipole moments, generally leading to greater values of $\delta_{2PA}$ due to enhanced ICT processes [66].

Single-Crystal X-Ray Structural Analysis

Single crystals for X-ray analysis were grown by the diffusion of hexane into a concentrated solution of **AXF-Al** in ethyl acetate. The central core of the molecule (Fig. 6) shows only slight deviation from planarity. The revealed planarity of the

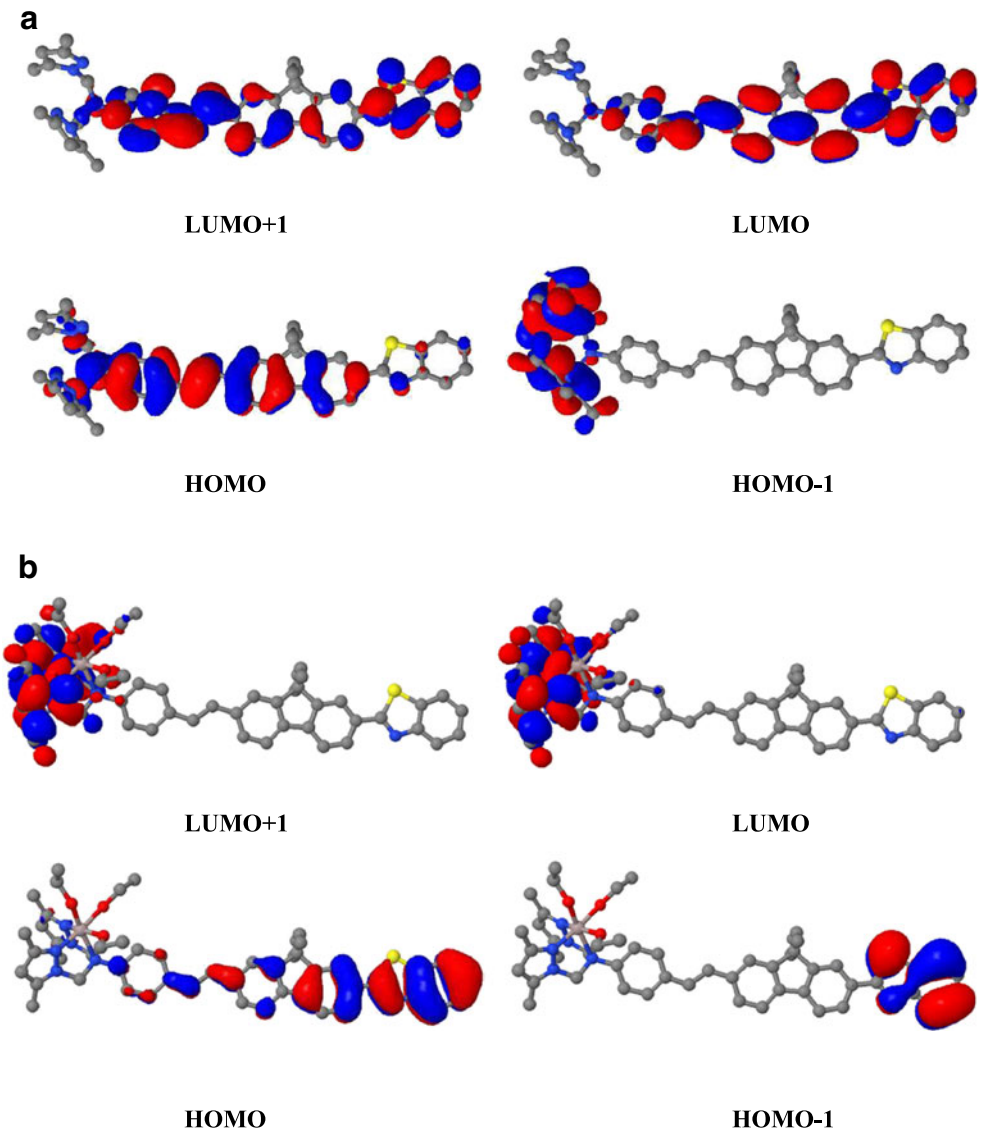


**Fig. 8** Isosurface plots of the HOMO-1, HOMO, LUMO, and LUMO+1 for **AXF-Al** (**a**) and the probe-aluminum complex (**b**)

benzathiazole-fluorene-styryl unit suggests strong conjugation within the central molecular core. The ethyl substituents on both sides of the fluorene moiety prevent significant overlap of fluorene fragments in the crystal. However, some side overlap with a distance between the main planes of fluorene fragments equal to 3.289 Å is observed, suggesting the possibility of π-π intermolecular interactions in the crystal. Attention is drawn to the aniline pyrazolyl unit. The C(30)-N(2) bond of the aniline is 1.408 Å, which indicates the donation of N lone pairs to the delocalized system [67].

### Quantum Chemical Calculations

The molecular geometries of the ligand and its $Al^{3+}$ complex were optimized at the B3LYP/6-311G* level in the density functional theory (DFT) formalism using the GAUSSIAN 09 program package [68] to study the effect of the nature of the ligand in the metal complex on 2PA properties. The geometries corresponding to global minima, obtained with the semi-empirical AM1 method, were similar to DFT results.

To gain insight into the effects of $Al^{3+}$ on the 2PA properties of the chromophore, quantum chemical calculations were performed for a model of the ligand as a metal–ligand complex model, excluding the non-coordinating perchlorate for simplicity. The model complex was based upon proposed tridentate coordination of the ligand via the aniline nitrogen and the two vacant nitrogens on the pyrazoles and three solvent (EtOH) molecules.

The optimized geometries obtained for the ligand corresponded to results obtained from the single crystal x-ray analysis (Fig. 6). The aniline C-N distance of the ligand in the calculated model, 1.421 Å, is in agreement with what was found in the crystal structure, 1.408 Å. In the calculated complex, there is an increase of this bond length to 1.502 Å, indicating perturbation of the N's donating ability upon ligating to metal. The model complex provides favorable molecular geometry as the Al–N(pz) distances were 1.976 and 2.033 Å, in the range of a normal coordinated heterocyclic Al–N bond [69] while the Al–N(aniline) bond of 2.211 Å is within literature tolerance [70].

Generally, the frontier molecular orbitals, especially HOMO−1, HOMO, LUMO, and LUMO+1, make important contributions to electronic transition in both single- and two-photon excitation. In Figs. 7 and 8, the contours of the non-degenerate HOMO−1, HOMO, LUMO, and LUMO+1 for the ligand and its Al complex are shown. We tentatively assign the HOMO-LUMO transition in the contour diagrams as the $\pi \rightarrow \pi^*$ transition of the chromophore. Upon complexation, the HOMO–LUMO transition can be thought to be a reflection of the intra-ligand charge transfer (ILCT).

In the contour maps of the ligand, both the HOMO and the HOMO-1 show a significant electronic contribution on the donor side of the molecule, which is in agreement with the high electron-donating ability of the aniline unit with minimal contribution from the benzothiazole. In comparing the energy level diagrams of the ligand and its complex with the Al(III) ion, it is found that complexation results in an inversion of the position of the HOMO and LUMO. The electron density of the LUMO is now centered around the acidic metal center, while that of the HOMO is predominantly lying on the benzothiazole unit. From the perspective of the HOMO of the ligand as well as Al complex, it can be concluded that electron donation from the amino nitrogen is sufficiently reduced in the metal complex.

## Conclusions

We have successfully synthesized and comprehensively characterized the fluorene-based aluminum probe **AXF-Al**, which offers a ratiometric means for the fluorometric analysis of $Al^{3+}$ in the ppb range. Up-converted emission via 2PA of the probe and $Al^{3+}$ complex was demonstrated. This means that this probe has a very high fluorescent imaging selectivity to $Al^{3+}$ among a number of common metal ions. Theoretical calculations carried out at the B3LYP/6-311G* level in the density functional theory (DFT) formalism show optimized geometry consistent with the crystal structure, and upon metal binding, there is nominal change in the value of $\delta_{2PA}$ cross section in the metal complexes. Significantly, this new probe exhibited selectivity for $Al^{3+}$ relative to a number of other common metal cations.

**Acknowledgments** The National Science Foundation (CHE-0832622, CHE-0840431, and DMR-0934212) and the National Academy of Sciences (PGA-P210877) are gratefully acknowledged for support of this work.

## References

1. Exley C (1999) A molecular mechanism of aluminium-induced Alzheimer's disease? J Inorg Biochem 76:133–140
2. Verstraeten S, Aimo L, Oteiza P (2008) Aluminium and lead: molecular mechanisms of brain toxicity. Arch Toxicol 82:789–802
3. Exley C (2001) Aluminium and Alzheimer's disease: the science that describes the link. Elsevier, Amsterdam
4. Golub MS, Domingo JL (1996) What we know and what we need to know about developmental aluminum toxicity. J Toxicol Environ Health 48:585–597
5. Gonda Z, Lehotzky K, Miklosi A (1996) Neurotoxicity induced by prenatal aluminum exposure in rats. Neurotoxicology 17:459–470
6. Anane R, Creppy EE (2001) Lipid peroxidation as pathway of aluminium cytotoxicity in human skin fibroblast cultures: prevention by superoxide dismutase+catalase and vitamins E and C. Hum Exp Toxicol 20:477–481
7. Hellstroem H-O, Mjoeberg B, Mallmin H, Michaelsson K (2005) The aluminum content of bone increases with age, but is not higher in hip fracture cases with and without dementia compared to controls. Osteoporos Int 16:1982–1988

8. Li X, Zhang L, Zhu Y, Li Y (2011) Dynamic analysis of exposure to aluminum and an acidic condition on bone formation in young growing rats. Environ Toxicol Pharmacol 31:295–301
9. Gruber W, Herbauts J (1990) Determination of aluminum in the presence of high concentrations of dissolved salts by atomic absorption spectrometry. Analusis 18:12–15
10. Quinonero J, Mongay C, de la Guardia M (1991) Determination of aluminum at the parts per billion level by solvent extraction and flame atomic emission spectrometry. Microchem J 43:213–221
11. Sancho D, Deban L, Campos I, Pardo R, Vega M (2000) Determination of nickel and cobalt in refined beet sugar by adsorptive cathodic stripping voltammetry without sample pretreatment. Food Chem 71: 139–145
12. Li Y-G, Li H-J (2010) Determination of trace aluminum (III) by fluorescence spectrophotometry with ciprofloxacin. Chin J Spectrosc Lab 27:1339–1342
13. Jiang C, Tang B, Fu H, Wang R (1997) Determination of aluminum using new fluorescent derivatives of salicylaldehyde hydrazone. Huaxue Shiji 19:353–355
14. Wang L, Liu J, Wang L, Xu F, Cheng H (2003) Preparation and application of a novel fluorescent nanoparticle as aluminum fluorescence probe. Anal Lett 36:1621–1629
15. Nguyen DM, Frazer A, Rodriguez L, Belfield KD (2010) Selective fluorescence sensing of zinc and mercury ions with hydrophilic 1,2,3-triazolyl fluorene probes. Chem Mater 22:3472–3481
16. Belfield KD, Bondar MV, Frazer A, Morales AR, Kachkovsky OD, Mikhailov IA, Masunov AE, Przhonska OV (2010) Fluorene-based metal-ion sensing probe with high sensitivity to $Zn^{2+}$ and efficient two-photon absorption. J Phys Chem B 114:9313–9321
17. Nguyen DM, Wang X, Ahn H-Y, Rodriguez L, Bondar MV, Belfield KD (2010) Novel hydrophilic bis(1,2,3-triazolyl)fluorenyl probe for in vitro zinc ion sensing. ACS Appl Mater Interfaces 2:2978–2981
18. Matsui A, Umezawa K, Shindo Y, Fujii T, Citterio D, Oka K, Suzuki K (2011) A near-infrared fluorescent calcium probe: a new tool for intracellular multicolour Ca2+ imaging. Chem Commun 47:10407–10409
19. Prodi L, Bolletta F, Montalti M, Zaccheroni N (2000) Luminescent chemosensors for transition metal ions. Coord Chem Rev 205:59–83
20. Okamoto A, Ichiba T, Saito I (2004) Pyrene-labeled oligodeoxynucleotide probe for detecting base insertion by excimer fluorescence emission. J Am Chem Soc 126:8364–8365
21. Minta A, Kao JPY, Tsien RY (1989) Fluorescent indicators for cytosolic calcium based on rhodamine and fluorescein chromophores. J Biol Chem 264:8171–8178
22. Goppert-Mayer M (1931) Elementary processes with two quantum jumps. Ann Phys (Berlin, Ger) 9:273–294
23. Xu C, Zipfel W, Shear JB, Williams RM, Webb WW (1996) Multiphoton fluorescence excitation: new spectral windows for biological nonlinear microscopy. Proc Natl Acad Sci U S A 93:10763–10768
24. Kim JS, Kim HJ, Kim HM, Kim SH, Lee JW, Kim SK, Cho BR (2006) Metal ion sensing novel calix[4]crown fluoroionophore with a two-photon absorption property. J Org Chem 71:8016–8022
25. Pond SJK, Tsutsumi O, Rumi M, Kwon O, Zojer E, Bredas J-L, Marder SR, Perry JW (2004) Metal-ion sensing fluorophores with large two-photon absorption cross sections: aza-crown ether substituted donor-acceptor-donor distyrylbenzenes. J Am Chem Soc 126:9291–9306
26. Oheim M, Michael DJ, Geisbauer M, Madsen D, Chow RH (2006) Principles of two-photon excitation fluorescence microscopy and other nonlinear imaging approaches. Adv Drug Deliv Rev 58:788–808
27. Belfield KD, Schafer KJ, Liu Y, Liu J, Ren X, Van SEW (2000) Multiphoton-absorbing organic materials for microfabrication, emerging optical applications and non-destructive three-dimensional imaging. J Phys Org Chem 13:837–849
28. Morales AR, Schafer-Hales KJ, Marcus AI, Belfield KD (2008) Amine-reactive fluorene probes: synthesis, optical characterization, bioconjugation, and two-photon fluorescence imaging. Bioconjug Chem 19:2559–2567
29. Morales AR, Belfield KD, Hales JM, Van Stryland EW, Hagan DJ (2006) Synthesis of two-photon absorbing unsymmetrical fluorenyl-based chromophores. Chem Mater 18:4972–4980
30. Belfield KD, Schafer KJ, Mourad W, Reinhardt BA (2000) Synthesis of new two-photon absorbing fluorene derivatives via Cu-mediated ullmann condensations. J Org Chem 65:4475–4481
31. Trofimenko S (1986) The coordination chemistry of pyrazole-derived ligands. Prog Inorg Chem 34:115–210
32. Trofimenko S (1993) Recent advances in poly(pyrazolyl)borate (scorpionate) chemistry. Chem Rev 93:943–980
33. Pettinari C, Cingolani A, Lobbia GG, Marchetti F, Martini D, Pellei M, Pettinari R, Santini C (2004) Copper and silver derivatives of scorpionates and related ligands. Polyhedron 23:451–469
34. Pettinari C, Santini C (2003) 1.10–polypyrazolylborate and scorpionate ligands. In: Editors-in-Chief: JAM, Meyer TJ (eds) Comprehensive coordination chemistry II. Pergamon, Oxford, pp 159–210
35. Fujisawa K, Okamoto K (2007) Third generation of scorpionate ligands. Kagaku (Kyoto, Jpn) 62:64–65
36. Smith JM (2008) Strongly donating scorpionate ligands. Comment Inorg Chem 29:189–233
37. Eichhorn DM (2009) Janus scorpionates: supramolecular tectons for the directed assembly of hard-soft alkali metallopolymer chains. A second-generation Janus scorpionate ligand: controlling coordination modes in iron(II) complexes by steric modulation. Chemtracts 22: 135–140
38. Radi S, Attayibat A, Ramdani A, Lekchiri Y, Hacht B, Bacquet M, Morcellet M (2007) C, N-pyridylpyrazole-based ligands: synthesis and preliminary use in metal ion extraction. Sep Sci Technol 42: 3493–3501
39. Malek F, Ramdani A, Zidane I, Yahyi A, Radi S (2005) Tetrapyrazolic tripods. Synthesis and preliminary use in metal ion extraction. Tetrahedron 61:2995–2998
40. Zhao M, Samoc M, Prasad PN, Reinhardt BA, Unroe MR, Prazak M, Evers RC, Kane JJ, Jariwala C, Sinsky M (1990) Studies of third-order optical nonlinearities of model compounds containing benzothiazole, benzimidazole and benzoxazole units. Chem Mater 2:670–678
41. Kannan R, He GS, Yuan L, Xu F, Prasad PN, Dombroskie AG, Reinhardt BA, Baur JW, Vaia RA, Tan L-S (2001) Diphenylaminofluorene-based two-photon-absorbing chromophores with various $\pi$-electron acceptors. Chem Mater 13:1896–1904
42. Kosugi M, Koshiba M, Atoh A, Sano H, Migita T (1986) Palladium-catalyzed coupling between organic halides and organotin compounds involving carbon-nitrogen unsaturated bonds at the reaction centers. Bull Chem Soc Jpn 59:677–679
43. Shriver DF, Drezdzon MA (1986) The manipulation of air-sensitive compounds. Wiley
44. Armarego WLF, Chai CLL. Purification of laboratory chemicals, 6th edn. Elsevier
45. Lakowicz JR (1999) Principles of fluorescence spectroscopy. Kluwer, New York
46. Xu C, Webb WW (1996) Measurement of two-photon excitation cross sections of molecular fluorophores with data from 690 to 1050 nm. J Opt Soc Am B 13:481–491
47. Belfield KD, Bondar MV, Przhonska OV, Schafer KJ (2002) Steady-state spectroscopic and fluorescence lifetime measurements of new two-photon absorbing fluorene derivatives. J Fluoresc 12:449–454
48. Belfield KD, Bondar MV, Przhonska OV, Schafer KJ, Mourad W (2002) Spectral properties of several fluorene derivatives with potential as two-photon fluorescent dyes. J Lumin 97:141–146
49. Belfield KD, Bondar MV, Przhonska OV, Schafer KJ (2002) Photophysical characterization of 2,9-bis(7-benzothiazole-9,9'-didecylfluoren-2-yl)perylene diimide: a new standard for steady-state fluorescence anisotropy. J Photochem Photobiol A 151:7–11

50. Albota MA, Xu C, Webb WW (1998) Two-photon fluorescence excitation cross sections of biomolecular probes from 690 to 960 nm. Appl Opt 37:7352–7356
51. Benesi HA, Hildebrand JH (1949) A spectrophotometric investigation of the interaction of iodine with aromatic hydrocarbons. J Am Chem Soc 71:2703–2707
52. Connors KA (1987) Binding constants: the measurement of molecular complex stability. Wiley
53. Valeur B (2001) Fluorescent molecular sensors of ions and molecules. In: Molecular fluorescence. Wiley-VCH Verlag GmbH, pp 273–350
54. Belfield KD, Morales AR, Kang B-S, Hales JM, Hagan DJ, Van SEW, Chapela VM, Percino J (2004) Synthesis, characterization, and optical properties of new two-photon-absorbing fluorene derivatives. Chem Mater 16:4634–4641
55. Horner L, Hoffman H, Wippel HG, Klahre G (1959) Phosphorus organic compounds. XX. Phosphine oxides as reagents for olefin formation. Chem Ber 92:2499–2505
56. Wadsworth WS Jr, Emmons WD (1961) The utility of phosphonate carbanions in olefin synthesis. J Am Chem Soc 83:1733–1738
57. Jiang Z, Deng R, Tang L, Lu P (2008) A new fluorescent chemosensor detecting $Zn^{2+}$ and $Cu^{2+}$ in methanol/HEPES buffer solution. Sensors Actuators B Chem 135:128–132
58. Wang J, Qian X, Cui J (2006) Detecting $Hg^{2+}$ ions with an ICT fluorescent sensor molecule: remarkable emission spectra shift and unique selectivity. J Org Chem 71:4308–4311
59. Videva V, Chauvin A-S, Varbanov S, Baux C, Scopelliti R, Mitewa M, Buenzli J-CG (2004) Cobalt(II), nickel(II), copper(II), and zinc(II) complexes with a p-tert-butylcalix[4]arene fitted with phosphinoyl pendant arms. Eur J Inorg Chem 2173–2179
60. Birjees BS, Memon S, Mahroof TM, Bhanger MI (2008) Synthesis, characterization and investigation of antioxidant activity of cobalt-quercetin complex. J Mol Struct 892:39–46
61. Chen Z, Schall OF, Alcala M, Li Y, Gokel GW, Echegoyen L (1992) Unusual 1:2 ligand:metal complex formation between an anthraquinone cryptand and lithium(+). J Am Chem Soc 114:444–451
62. Tolosa J, Zucchero AJ, Bunz UHF (2008) Water-soluble cruciforms: response to protons and selected metal ions. J Am Chem Soc 130: 6498–6506
63. Morales AR, Schafer-Hales KJ, Yanez CO, Bondar MV, Przhonska OV, Marcus AI, Belfield KD (2009) Excited state intramolecular proton transfer and photophysics of a new fluorenyl two-photon fluorescent probe. ChemPhysChem 10:2073–2081
64. Belfield KD, Bondar MV, Yanez CO, Hernandez FE, Przhonska OV (2009) Two-photon absorption and lasing properties of new fluorene derivatives. J Mater Chem 19:7498–7502
65. Sumalekshmy S, Henary MM, Siegel N, Lawson PV, Wu Y, Schmidt K, Brédas J-L, Perry JW, Fahrni CJ (2007) Design of emission ratiometric metal-ion sensors with enhanced two-photon cross section and brightness. J Am Chem Soc 129:11888–11889
66. Das S, Nag A, Sadhu KK, Goswami D, Bharadwaj PK (2007) Metal induced enhancement of fluorescence and modulation of two-photon absorption cross-section with a donor-acceptor-acceptor-donor receptor. J Organomet Chem 692:4969–4977
67. Gross KC, Seybold PG (2000) Substituent effects on the physical properties and pKa of aniline. Int J Quantum Chem 80:1107–1115
68. Frisch MJ, Trucks GW, Schlegel HB, Scuseria GE, Robb MA, Cheeseman JR, Scalmani G, Barone V, Mennucci B, Petersson GA, Nakatsuji H, Caricato M, Li X, Hratchian HP, Izmaylov AF, Bloino J, Zheng G, Sonnenberg JL, Hada M, Ehara M, Toyota K, Fukuda R, Hasegawa J, Ishida M, Nakajima T, Honda Y, Kitao O, Nakai H, Vreven T, Montgomery JA, Peralta JE, Ogliaro F, Bearpark M, Heyd JJ, Brothers E, Kudin KN, Staroverov VN, Kobayashi R, Normand J, Raghavachari K, Rendell A, Burant JC, Iyengar SS, Tomasi J, Cossi M, Rega N, Millam JM, Klene M, Knox JE, Cross JB, Bakken V, Adamo C, Jaramillo J, Gomperts R, Stratmann RE, Yazyev O, Austin AJ, Cammi R, Pomelli C, Ochterski JW, Martin RL, Morokuma K, Zakrzewski VG, Voth GA, Salvador P, Dannenberg JJ, Dapprich S, Daniels AD, Farkas, Foresman JB, Ortiz JV, Cioslowski J, Fox DJ (2009) Gaussian 09, revision A.02. Wallingford CT
69. Yu Z, Wittbrodt JM, Xia A, Heeg MJ, Schlegel HB, Winter CH (2001) Hydrogen and dihydrogen bonding as important features of the reactivity of the bridging hydride in pyrazolate-bridged dialuminum complexes. Organometallics 20:4301–4303
70. Willcocks AM, Gilbank A, Richards SP, Brayshaw SK, Kingsley AJ, Odedra R, Johnson AL (2011) Synthesis and structure of 6-aminofulvene-2-aldiminate complexes. Inorg Chem 50:937–948